Partition-Based Extraction of Cerebral Arteries from CT Angiography with Emphasis on Adaptive Tracking

Hackjoon Shim[1], Il Dong Yun[2], Kyoung Mu Lee[1], and Sang Uk Lee[1]

[1] School of Electrical Engineering and Computer Science,
Seoul National University, Seoul, 151-742, Korea
hjshim@diehard.snu.ac.kr, kmlee@ee.snu.ac.kr, sanguk@ipl.snu.ac.kr
[2] School of Electronics and Information Engineering,
Hankuk University of Foreign Studies, Yongin, 449-791, Korea
yun@hufs.ac.kr

Abstract. In this paper a method to extract cerebral arteries from computed tomographic angiography (CTA) is proposed. Since CTA shows both bone and vessels, the examination of vessels is a difficult task. In the upper part of the brain, the arteries of main interest are not close to bone and can be well segmented out by thresholding and simple connected-component analysis. However in the lower part the separation is challenging due to the spatial closeness of bone and vessels and their overlapping intensity distributions. In this paper a CTA volume is partitioned into two sub-volumes according to the spatial relationship between bone and vessels. In the lower sub-volume, the concerning arteries are extracted by tracking the center line and detecting the border on each cross-section. The proposed tracking method can be characterized by the adaptive properties to the case of cerebral arteries in CTA. These properties improve the tracking continuity with less user-interaction.

1 Introduction

The wall of a cerebral artery may become weak and have a bulging spot like a thin balloon. This is an aneurysm inside which the flowing blood can rupture the weakened wall and result in a subarachnoid hemorrhage (SAH). However, most people with unruptured aneurysms have no symptoms. The overall annual risk of rupture of an intact intracranial aneurysms is 1.9%[1]. Therefore, periodical screening by medical images is considerably required for potential patients.

As the imaging technology develops, the resolution becomes higher, but at the same time, the amount of data becomes enormous increasing the burdens of the experts examining vessels and the associated pathologies. For prognosis of SAH it is crucial to examine the vascular structure exactly not hindered by bone or vein. If only the vascular structure can be segmented out in CTA, it will be very helpful for prognosis or surgery planning.

G.E. Christensen and M. Sonka (Eds.): IPMI 2005, LNCS 3565, pp. 357–368, 2005.

The most basic method for segmentation is the combination of thresholding and connected-component analysis (CCA)[2]. However, being applied to the segmentation of cerebral arteries from bone or vein in CTA, it has some problems mainly due to the following two facts. One is the overlapping intensity distributions of bone and vessels making thresholding not effective. The other is the close contact between arteries and bone or vein resulting in the infeasibility of CCA. Bone usually has higher intensity values than arteries. However the partial volume effect (PVE)[3] causes in-between voxels to have in-between intensity values so that the intensity distributions of bone and arteries overlap with each other. Veins have only a little lower intensity values than arteries and are very close to arteries.

To settle these problems it is required to make use of some prior information or anatomic knowledge about arteries like follows:

- Vessels are smoothly varying structures with nearly circular or elliptical cross-sections.
- In the cranial cavity the arteries of main interest flow apart from bone. However below the floor of the cranial cavity the arteries often pass through bone.

Until now a number of papers have been published on the vessel extraction in magnetic resonance angiography (MRA) [4, 5, 6]. MRA does not show bone which makes vessel extraction more easily than CTA. As for CTA only a few researches have been performed.

Suryanarayanan *et. al* [8] took account of the profiles of bone and sinus (cavity) and partitioned the head volume into three sub-volumes. Each sub-volume has a consistent spatial relationship between bone and vessels enabling separate segmentation algorithm to be applied. This work is not on segmentation itself but on the proper partitioning of volumes for segmentation.

Wink *et. al* [9] extracted the abdominal aorta based on tracking of the center line. The abdominal aorta is thick and mostly straight, consequently much simpler to extract than cerebral arteries. Their method is very similar to the proposed method in this paper. However, in being applied to the case of cerebral arteries in CTA, consideration of obscure boundary of arteries, especially to bone or vein was not sufficiently. The proposed method adds some adaptive properties to the extraction of cerebral arteries in CTA. Its better performance in tracking will be confirmed by some experiments in section 3.

Hong *et. al* [10] eliminated bone in brain with two CT volumes scanned before and after the injection of contrast dye, respectively. They performed rigid registration between the two CT volumes and subtracted the pre-contrast volume from the post-contrast volume. This work belongs to a digital subtraction angiography (DSA) and can make a perfect extraction theoretically. The drawback of this approach is that it requires twice of scanning which doubles the burden and cost for patients.

The outline of this paper is as follows. In section 2 the overall workflow of the proposed method will be explained. In section 3 the experimental results and the analysis will be provided. And finally we will conclude with section 4.

2 Description of the Overall Workflow

This paper proposes a method to extract cerebral arteries from CTA. The overall workflow is composed of the following five sub-sections. First, a CT data is acquired, re-sampled and pre-processed. Then the head CT volume is partitioned into two sections each of which has a consistent spatial relationship between bone and vessels. To each sub-volume a separate segmentation algorithm is applied. Therefore the next two sub-sections describe these two algorithms, repectively. Finally, to remove the discontinuities between the sub-volumes, the inter-partition tracking is devised and will be explained in the last sub-section.

2.1 Data Acquisition and Pre-processing

A CT data is sampled in an anisotropic space, where the resolution in each of x-, y-, and z-directions is not equal. For further processing of volume data, we interpolated the intensity value on each grid in the z-direction by trilinear interpolation. To suppress the effects of noise and artifacts, the isotropically resampled volume is pre-processed by the convolution with a Gaussian kernel.

2.2 Partitioning of a Head CT Volume

In the cranium, the arteries of main interest are called as the Circle of Willis and aneurysms usually happen on the Circle of Willis located on the floor of the cranial cavity. The cranial cavity corresponds to the upper part of the head CT volume data, and has the concerned arteries separated far away from bone. In the while, below the floor of the cranial cavity, the arteries often pass through bone and run closely to vein. As mentioned earlier, these circumstances produce obscure boundaries of the arteries which require special treatment of the lower sub-volume.

If we consider the profile of bone, in the upper sub-volume, bone forms an outer boundary as in Fig. 1 (a). As we go down, bone approaches closer to the inner arteries and consequently constitutes a complex structure as seen in Fig. 1 (b). We assume a square region on each slice as in Fig. 1 (c). From the top of the head the ratio r_{bone} of the number of bone voxels in the square to the total number of voxels in the square is computed on each slice. At first no bone voxels can be found, but as we go down, the number of bone voxels increases and the slice where it exceeds a threshold t_{bone} is the partitioning slice. Empirically t_{bone} is set to 0.002.

2.3 Extraction in the Upper Sub-volume (Threshold-Morphological Method)

As bone and vessels are not adjacent to each other in the upper sub-volume, they can be well separated mostly by intensity thresholds and CCA. On the contrary as stated in the introduction, the PVE produces voxels of in-between intensity values on the boundary of the bone structure. These voxels are what should have

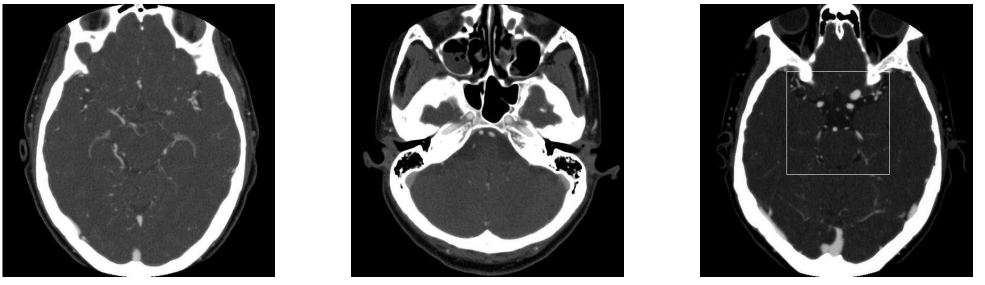

(a) (b) (c)

Fig. 1. Bone voxel distributions in : (a) A slice of the upper sub-volume, (b) a slice of the lower sub-volume, (c) The partitioning slice

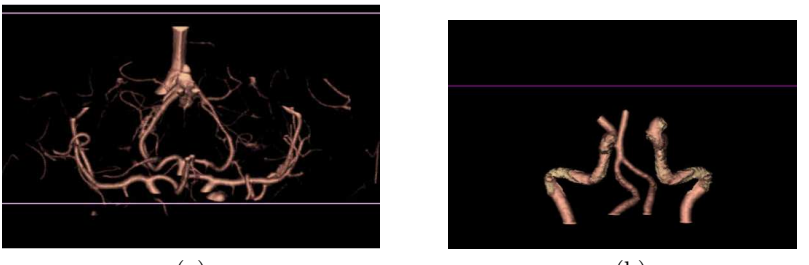

(a) (b)

Fig. 2. Vessels extracted: (a) In the upper sub-volume, (b) In the lower sub-volume

been removed together with bone structure. Thus, we applied morphological dilation operation with the ball-shaped structuring element to add these voxels to the bone structure. Next, after the application of CCA, only the components which satisfies the size and the shape criteria remain as vessel segments. The size criterion is that the size of a component should be larger than a threshold t_{size} and the shape one is that the component has a saturation value less than another threshold t_{sat}. Saturation is a compactness measure being the ratio of the number of voxels in the component to the number of voxels in the bounding box of the component. Empirically, t_{size} t_{sat} are 100 and 0.1, respectively.

Fig. 2 (a) shows the vessels extracted by the method in the upper sub-volume. The upper part of the Circle of Willis can be examined clearly with the bone structure removed. Some veins are visualized together, but they can be removed by a simple post-processing using some anatomical knowledge.

2.4 Extraction in Lower Partition (Adaptive Tracking Method)

In the lower sub-volume, as the arteries are often adjacent to bone or veins, they could not be segmented out only by intensity information. In this paper, the main arteries are extracted by tracking the central axes and detecting the border

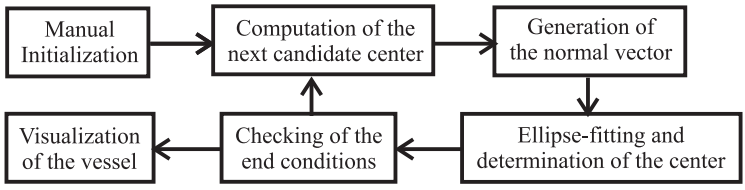

Fig. 3. The block diagram of the segmentation in the lower sub-volume

points on each cross-section. The tracking method in the lower sub-volume is composed of several step as shown in Fig. 3. The most important steps are the ones of "Generation of the normal vector" and "Ellipse-fitting and determination of the center".

Manual Initialization and Computation of the Next Candidate Center: The tracking is initialized by the user designating a center point and a normal vector. The arteries of main interest are left-right internal carotid arteries (ICA) and left-right vertebral arteries (VA), consequently four pairs of an initial center and an initial normal vector are required.

The candidate center for the next cross-section $\boldsymbol{C}_{cand}$ is computed by adding the step vector $\boldsymbol{b}$ to the previous center $\boldsymbol{C}_{last}$. The step vector $\boldsymbol{b}$ is in the same orientation of the normal vector computed for the last cross-section.

Generation of the Normal Vector: As seen in Fig. 4, vessels are assumed to be cylinders, and the direction of vessel axis and the area of its perpendicular cross-section are denoted by $\boldsymbol{n_0}$ and S_0, respectively at the center O. Then, an arbitrary cross-section with the angle of ϕ has its area S of (1). Consequently the perpendicular cross-section is determined by minimizing S which means that $\phi = 0$.

$$S = \frac{S_0}{\cos\phi}, \qquad 0 \leq \phi \leq \frac{\pi}{2}. \tag{1}$$

However the real vessel is generally not a cylinder. Therefore to minimize the cross-section area, both of θ and ϕ of the spherical coordinate system should

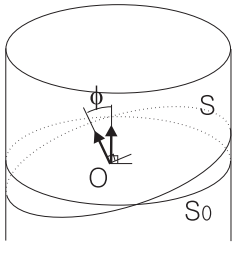

Fig. 4. Cross-sections and their normal vectors

be sampled in uniform intervals as (2) and (3). θ is the azymuthal angle in the xy-plane from the x-axis with $0 \leq \theta \leq 2\pi$ and ϕ is the zenith angle from the z-axis with $0 \leq \phi \leq \frac{\pi}{2}$[11].

$$\Theta = \{\theta_i \;\Big|\; \theta_i = 2\pi \frac{i}{M}, \quad i = 0, \ldots, M-1\}. \tag{2}$$

$$\Phi = \{\phi_j \;\Big|\; \phi_j = \frac{\pi}{2} \frac{j}{N}, \quad j = 0, \ldots, N\}. \tag{3}$$

The normal vector, $\mathbf{n}$ is computed as (4) at the pair of (θ, ϕ).

$$\mathbf{n}(\theta, \phi) = (\cos\theta \sin\phi, \sin\theta \sin\phi, \cos\phi). \tag{4}$$

When we denote as $\mathbf{n}_{ij} = \mathbf{n}(\theta_i, \phi_j)$, the correct normal vector of the cross-section, $\mathbf{n}_{min} = \mathbf{n}(\theta_{i_{min}}, \phi_{j_{min}})$ is defined from (5).

$$(i_{min}, j_{min}) = \arg \min_{\substack{i \in \{0,\ldots,M-1\} \\ j \in \{0,\ldots,N\}}} S_{ij}, \tag{5}$$

where S_{ij} = *Area of the cross-section determined by* (θ_i, ϕ_j).

However S_{ij} can be calculated only after the border of the cross-section is correctly obtained over all the possible pair of (θ_i, ϕ_j). It is worth to note that if the detected border points are scattered sparsely, S_{ij} will be large and vice versa. Therefore we determine the normal vector by minimizing the variance of the positions of the border points instead of the area of the cross-section.

Ellipse-Fitting and Determination of the Center: At the cross-section perpendicular to the previous normal vector, the border points of the artery are detected and fitted to an ellipse. From the candidate center of the cross-section, rays are cast along the directions equally sampled around the candidate center as in Fig. 5 (d). The radial component of the gradient along each ray is plotted as in Fig. 6. Fig. 5 (a) and (d) show the usual case where the artery is surrounded only by normal tissues. The contrast-enhanced artery has higher intensity value than the surrounding tissues, so the border point along the ray is detected as the first negative extremum below some negative threshold t_-.

Fig. 5 (b) and (e) show the case where the artery passes through bone. Since bone has much higher intensity values that the artery, the plot of the radial gradient component shows large positive values. For this reason, we invert the sign of the negative threshold t_- into some positive value t_+ and detect the border point as the first positive extremum above t_+.

Finally Fig. 5 (c) and (f) are the case where the artery is adjacent to vein. As veins have similar intensity values to arteries resulting in a plain plot of the radial gradient component, we reduce the magnitude of t_-. With this smaller t_- the border point is detected.

Fig.5 (e) and (f) show the detected border points in these special cases. Although there are some outliers, the modified thresholds generally produce proper border points. These outliers should be removed in the ellipse-fitting

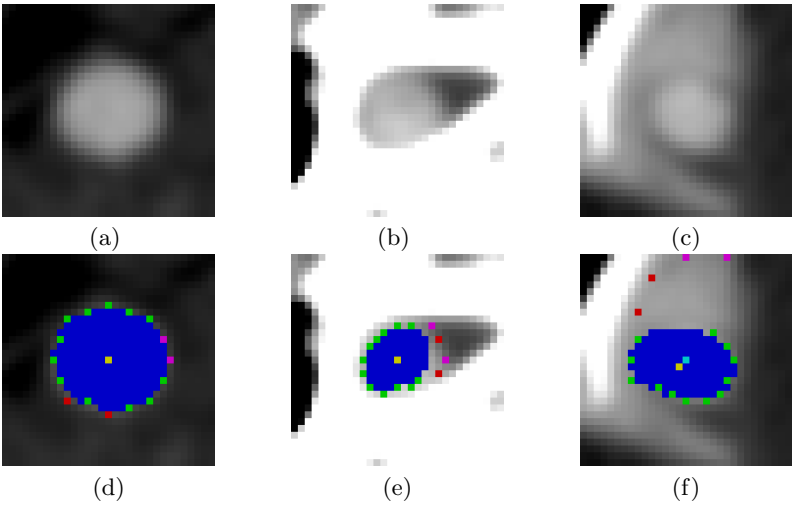

Fig. 5. Artery cross-sections : (a) Surrounded by only normal tissues, (b) Surrounded by bone structure, (c) Adjacent to vein, (d) (e) (f) The detected border points, the outliers, and the fitted ellipse of (a), (b), and (c), respectively

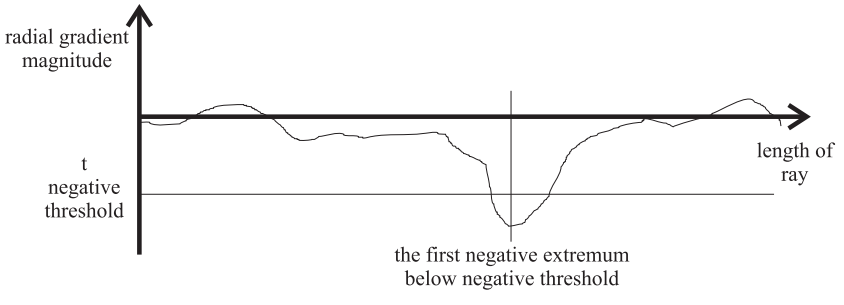

Fig. 6. The radial component of the gradient along a ray

which can be certified by the blue ellipse not effected by the outliers in Fig. 5 (e) and (f). The ellipse-fitting was implemented by the use of Intel OpenCV library[12].

The removal of outliers are performed by two separate processes. The first process is illustrated in Fig. 7 (a). E is the ellipse fitted in the previous cross-section and E_t is the translation of E by the amount of the step vector $\boldsymbol{b}$. Since arteries have smoothly varying structure as stated in the introduction, if the length of $\boldsymbol{b}$ is sufficiently small, the new boundary in the current cross-section will not be much different from E_t. Therefore, the border points which are the most distant from E_t are removed and are named as the absolute outliers denoted by 'o' in Fig. 7 (a). If n_{total} and n_{ao} denote the number of all the

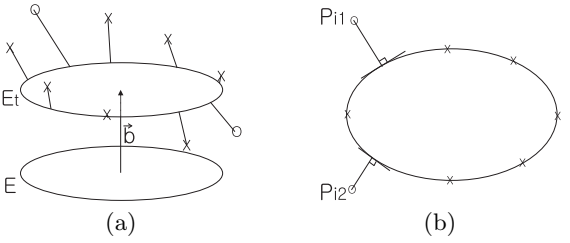

Fig. 7. Removal of outliers: (a) Absolute outliers, (b) Relative outliers

detected border points in a cross-section and the absolute outliers, respectively, the ratio $r_{ao} = n_{ao}/n_{total}$ can be adjusted according to the obscureness of the boundary. Next the relative outliers are removed among the remained border points as in Fig. 7 (b). If the number of the relative outliers is denoted by n_{ro}, the number of all the possible n_{ro}-tuples each of which is composed of n_{ro} points is $n_{tuple} = \binom{n_{total}-n_{ao}}{n_{ro}}$.

For each n_{ro}-tuple $T_i = \{P_{i1}, \ldots P_{in_{ro}}\}, \quad i = 1, \ldots, n_{tuple}$, an ellipse E_i is approximated using the rest border points except the points of T_i. If the 3D distance from a point P to the boundary of an ellipse E is denoted by $d(E, P)$, the sum of distances d_i of (6) measures how much each T_i will be taken as the relative outliers. ω_j is the weight for P_{ij} and empirically is set to 1 if P_{ij} is exterior to the ellipse E_i and set to 0.2 otherwise. This is for the purpose of weighting the exterior outliers more than the interior ones, because they produce larger errors in ellipse-fitting. Afterwards the points of T_i minimizing d_i are removed as the relative outliers.

$$d_i = \sum_{j=1}^{n_{ro}} \omega_j d(E_i, P_{ij}). \tag{6}$$

Checking of the End Conditions and Visualization of the Vessel: The possible end conditions can be the maximum length of the artery, the z-coordinate of the center point, or whether being out of the artery boundary. If the end condition is not satisfied, the workflow goes back to the stage of "To compute the next candidate center" of Fig. 3. Otherwise, the workflow terminates and the accumulated cross-sections will be visualized. Fig. 2 (b) shows left-right ICA's and left- right VA's. In spite of the varying diameter of the arteries and the overlapping intensity distributions, the proposed tracking scheme has extracted the main arteries effectively.

2.5 Inter-partition Tracking

The proposed method applies a separate segmentation algorithm to each sub-volume. This inevitably causes discontinuities on the partitioning slice between the two sub-volumes as in Fig. 8 (a). We perform the inter-partition tracking to

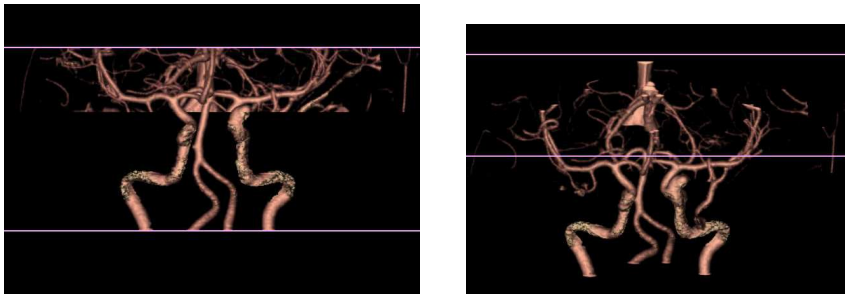

(a) (b)

Fig. 8. Inter-partition tracking to eliminate the discontinuities on the partitioning slice: (a) Before, (b) After

eliminate these discontinuities. First, 2-D CCA is executed on the partitioning slice. Among the connected components, only those that are large enough and in the region of interest are selected as the seeds for tracking. The central mean of each seed is the initial center point and the initial normal vector is downward to the lower sub-volume. From each seed the tracking is initiated to connect the discontinuities. Fig. 8 (b) is the result after the inter-partition tracking and shows that most of the discontinuities are eliminated.

3 Results and Discussion

We performed experiments with 24 data sets which were provided by a company and a hospital (not-specified due to anonymous reviewing). Three of them are the double-scanned data sets composed of before-injection, after-injection, and their DSA result. Let us call them as DS (double-scaned) data sets of from DS01 to DS03. The rest are the single-scanned volumes scanned after the injection and are named as from SS01 to SS21. Mainly concerned about the tracking in the lower sub-volume, we defined some subjective evaluation criterion. It designates a result as a success when at most one of the arteries of main interest is missed or cut with no re-initialization. According to this criterion 17 out 24 data sets marked as the success and the subjective success rate can be $70.83\% = 17/24$.

3.1 Adaptiveness of the Proposed Tracking

To evaluate the proposed tracking method more objectively, we performed experiments with the left ICA of DS03 data set. The most important measure about the tracking performance can be the ability to continue tracking without getting astray or making turnovers which requires user's re-initialization. We counted the number of requirements for re-initialization (in short, NRR) as the sum of the number of getting astray (NGA) and the number of turnovers (NTO). For tracking to get astray means that the new center point is out of

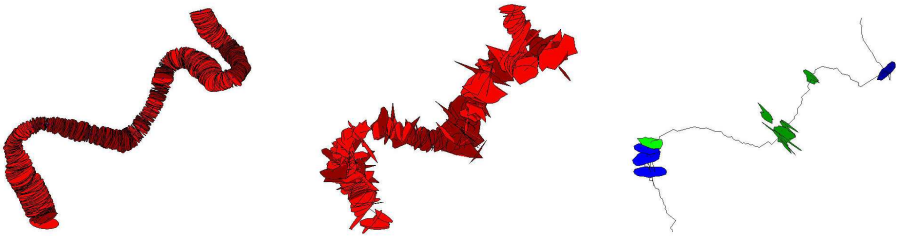

(a) (b) (c)

Fig. 9. Left ICA : (a) The cross-sections tracked by the proposed method, (b) The cross-sections tracked by a conventional method[9], (c) The cross-sections re-initialized by the user in the conventional method[9] with the green ones owing to getting astray and the blue ones owing to turnovers, repectively

the true artery boundary. Fig. 9 (a) shows the tracking result of the proposed method by the accumulated cross-sections. It required no re-initialization, i.e. $NRR = NGA + NTO = 0$.

On the contrary, Fig. 9 (b) is the cross-sections by the tracking method[9] using the center-likelihood (CL) measure for determining the new center point on a cross-section This method[9] was targeted for the abdominal aorta which is simpler to extract than the cerebral arteries. It used the difference between the last two center points for the generation of the step vector and provided not enough consideration to deal with outliers. Hence it is not appropriate for the extraction of the cerebral arteries as shown in Fig. 9 (b). When the left ICA passes through bone or is adjacent to veins, the border points are not exactly detected making the cross-sections irregular. Besides, in Fig. 9 (c), the green cross-sections are the re-initialized ones owing to getting astray and the blue ones indicate the re-initialization owing to turnovers. In this case, $NGA = 8$ and $NTO = 4$.

This comparison illustrates the adaptiveness of the proposed tracking which is due to the following facts.

- The normal vector at each cross-section is determined by minimizing all the cross-sections computed by the sampled pairs of (θ, ϕ).
- The gradient threshold is modified in the case where the artery is adjacent to veins.
- The outliers in detecting border points on a cross-sections are removed by two separate processes.

3.2 Visual Comparison to DSA Results

Each of the DS data sets has three volumes. We call them, as Before-volume, After-volume, and DSA-volume[10], respectively. The vascular structure including arteries can be seen clearly in Fig. 10 (a), (c), and (e). However this result

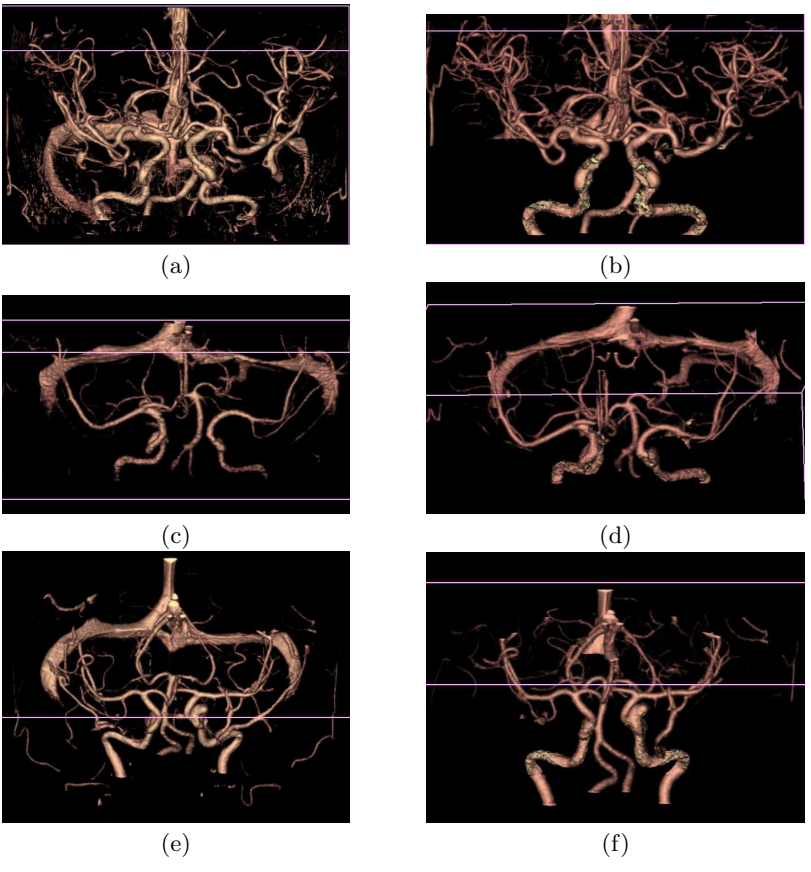

Fig. 10. Visual comparison to DSA results[10] : (a) (c) (e) The DSA results of DS01, DS02, and DS03, respectively, (b) (d) (f) The results of the proposed method of DS01, DS02, and DS03, repectively

requires double-scanning. The results of the proposed method are shown in Fig. 10 (b), (d), and (f) and are comparable to (a), (c), and (e).

The results of the proposed method show that where the arteries pass through bone, their surfaces are mixed with the colors of bone and vessel. This is inevitable when the segmentation result is being displayed using a bit-mask operation. Due to the PVE the voxel at the artery boundary adjacent to bone has higher intensity value than the normal artery surface voxel.

4 Conclusion

In this paper we proposed a method for the extraction of cerebral arteries in CTA. CTA also shows bone structure which hinders arteries to be seen. When

veins are adjacent to the arteries of interest, their spatial closeness and small intensity difference make the segmentation of arteries more difficult. The proposed method partitioned the CT volume into two sub-volumes and applied a separate segmentation algorithm to each segment. Specially, in the lower sub-volume, we added some adaptive properties to the simple tracking and they enhances the continuity of tracking in spite of the above difficulties. The experimental results confirmed that the proposed method had produced considerable amount of results which are subjectively satisfying and had enhanced the continuity of the tracking. The visual comparison to the DSA result illustrated that the proposed method is comparable to the result with double-scanned volumes which means a high applicability to the practical clinical use.

Acknowledgements. This research was supported by INFINITT Co. which also provided the data sets[13].

References

1. Rinkel, G.J.E., Djibuti, M. , Algra, A., Gijn, J.V., Prevalence and risk of rupture of intracranial aneurysms: a systematic review, Stroke, Vol. 29(1998), 251-256
2. Higgins, W.E., Spyra, W.J.T., Ritman, Automatic extraction of the arterial tree from 3-d angiograms, IEEE Conf. Eng. in Medicine and Bio., Vol. 2(1989) 563-564
3. Sonka, M., Fitzpatrick, J.M., Handbook of Medical Imaging, SPIE Press (2000)
4. Flasque, N., Desvignes, M., Constans, J., Revenu, M., Acquisition, segmentation, and tracking of the cerebral vascular tree on 3D magnetic resonance angiography images, Medical Image Analysis, Vol. 5(2001), 173-183
5. Sabry, M., Sites, C.B1., Farag, A.A., Hushek, S., A Fast Automatic Method for 3D Volume Segmentation of the Human Cerebrovascular, CARS (2002)
6. Wilson, D.L., Noble, J.A., An Adaptive Segmentation Algorithm for Time-of-flight MRA Dat, IEEE Trans. on Medical Imaging, Vol. 18(1999) 938-945
7. Chapman, B.E., Stapelton, J.O., Parker, D.L., Intracranial vessel segmentation from time-of-flight MRA using pre-processing of the MIP Z-buffer: accuracy of the ZBS algorithm, Medical Image Analysis, Vol. 8(2004) 113-126
8. Suryanarayanan, S., Mullick, R., Mallya, Y., Kamath, v., Automatic Partitioning of Head CTA for enabling Segmentation, SPIE Proceedings of Medical Imaging (2004)
9. Wink, O., Niessen, W.J., Viergever, M.A., Fast Delineation and Visualization of Vessels in 3-D Angiographic Images, IEEE Trans. on Medical Imaging, Vol. 19(2000) 337-346
10. Hong, H., Lee, H., Shin, Y.G., Seong, Y.H., Three-Dimensional Brain CT-DSA using Rigid Registration and Bone Masking for Early Diagnosis and Treatment Planning, Lecture Note on Artificial Intelligence 3378 (2004)
11. Zwillinger, D. (Ed.). Spherical Coordinates in Space, 4.9.9 in CRC Standard Mathematical Tables and Formulae, Boca Raton, FL: CRC Press (1995) 297-298
12. Open Source Computer Vision Library: Reference Manual, Intel Co. (2000)
13. http://www.infinitt.com/English/default.html